Pineda Jesús (Orcid ID: 0000-0002-5362-8614)

Response of small sharks to non-linear internal waves

Jesús Pineda[1], Sally Rouse[2], Victoria Starczak[1], Karl Helfrich[3] and David Wiley[4]

jpineda@whoi.edu Sally.Rouse@sams.ac.uk vstarczak@whoi.edu khelfrich@whoi.edu

david.wiley@noaa.gov

[1]Biology Department and [3]Physical Oceanography Department, Woods Hole Oceanographic Institution, Woods Hole, Massachusetts 02543, USA

[2]Scottish Association for Marine Science, Oban, Argyll, PA37 1QA, UK

[4]National Oceanic and Atmospheric Administration/Office of National Marine Sanctuaries, Stellwagen Bank National Marine Sanctuary, Scituate, Massachusetts, USA

Running Head: Sharks in Non-Linear Internal Waves

Keywords: Sharks, *Squalus acanthias*, distribution, depth distribution, vertical currents, behavior non-linear internal waves.

Abstract

Plankton and nekton may respond passively or actively to large-amplitude, non-linear internal waves (NLIW), with periods and wavelengths on the order of minutes and 100's of meters, and the NLIW can cause direct or indirect changes in distribution. NLIW are ubiquitous in the coastal ocean, but understanding the influence of NLIW on organism response and distribution is challenging, because of NLIW unpredictability, short temporal and spatial scales, and the difficulty in resolving the biological response. Measurements of currents, temperature, and shark acoustic traces in Massachusetts Bay were used to evaluate the short-term response of individuals, as well as the mean effects on the distribution of an aggregation of small sharks, *Squalus acanthias*. In two NLIW events, we detected 527 and 3,240 shark traces. Individuals moved up and down in response to the currents associated with the sinking and rising of the thermocline. However, mean distribution deepened during one of the events, suggesting that organisms did not merely move in concert with the thermocline oscillation, but that sharks instead may have responded actively. Measurements of vertical currents and shark's depth-change during one of the NLIW events indicate that with downward currents (sinking of the thermocline) the sharks tend to react passively. However, in response to the fastest upward currents, sharks appeared to swim down, supporting an active response in the rising phase of the wave. NLIW and other high-frequency processes can have a profound influence on the distribution of pelagic organisms, yet their ecological consequences remain largely unaccounted for.

Introduction

Understanding the distribution of animals in space and time is a fundamental goal of ecology. For species that are commercially exploited or vulnerable to disturbance from anthropogenic activities, such information is vital for the development of conservation strategies and management plans. In marine systems, the sharpest environmental gradients, including light, temperature, and stratification, align with the depth axis. Thus, the depth (vertical) distribution of individuals within the water column is an important component of a spatio-temporal distribution. Shark distribution is the result of active movement, but currents may also influence their distribution. Recent advances in sensor autonomy and miniaturization have revolutionized understanding of shark and other megafauna movement in the horizontal dimension (Hussey et al. 2015).

The depth distribution of shark species is not well known (Cortés et al. 2010), however. Studies using tags have addressed seasonal, lunar, and diel variability in vertical movement (Vianna et al. 2013). Positioning in the water column of sharks and other pelagic elasmobranchs is commonly interpreted as a response to thermal regulation, metabolic rate or as a result of foraging behavior (Sims et al. 2005). Little consideration has been given to the response of highly mobile pelagic predators to high-frequency variability (e.g., periods of seconds to few hours), despite such features influencing the energetic costs associated with swimming, or even the prey field. This gap is significant, because high frequency vertical variability caused by

internal waves and internal tides is pervasive in all oceans, and these phenomena can be a major structuring factor in coastal ecosystems, with effects ranging from nutrient input (Leichter et al. 2003), to larval transport (Pineda 1999) and prey aggregation (Greer et al. 2014),.

Two trains of internal waves generate semi-diurnally at low tide at Race Point channel, near the tip of Cape Cod, Massachusetts (Figure 1), propagating on average in two directions, 250°T and 275°T (da Silva and Helfrich 2008). Waves propagating 275° may approach the southwestern flank of Stellwagen Bank, which is ~10 km distant. SAR and in situ observations at the southwestern flank revealed NLIW consistent with Race Point origin in ~62-68% of cases, and wave trains had long crests (19 – 28 km), and a propagation speeds of 30 – 50 cm s^{-1} (da Silva and Helfrich 2008; Pineda et al. 2015). Because of the predictability of the NLIW at the southwestern flank, this site is ideal for investigating their ecological consequences. The occurrence of top predators at Stellwagen Bank southern flank is suggestive of the NLIW relevance (Chapter 4, U.S. Department of Commerce 2010).

Squalus acanthias (spiny dogfish) is a coastal, circumboreal species and the most abundant shark in the western North Atlantic (Bigelow and Schroeder 2002). Globally, the species is considered vulnerable by the IUCN and its population is declining (Fordham et al. 2006). It is slow growing, females reach maturity at 12 years (Nammack et al. 1985), and can live to at least 35 years old. Spiny dogfish are opportunistic predators on ctenophores, squid, bivalves, herring, hake, sand lance, and other benthic and pelagic invertebrates and fish (Link et al. 2002). *S. acanthias* are found in a range of water temperatures, with preferred temperatures in adults ranging from 6 to

13 °C (Shepherd et al. 2002; reviewed in Stehlik 2007). Tagged *S. acanthias* display day and night activity over a range of depths, including dives to over 600 m depths (Sulikowski et al. 2010). Offshore-onshore movement is related to water temperature and segregation of genders (Bigelow and Schroeder 2002), and aggregations migrate northward from North Carolina in the spring to Massachusetts and the Gulf of Maine (Jensen 1965).

We observed NLIW approaching Stellwagen Bank southwestern flank with measurements of currents, acoustic backscatter and temperature. Coincidentally, we detected aggregations of small sharks *Squalus acanthias* during two NLIW events. Analyses of these measurements were used to resolve shark individual and mean (aggregate) depth displacements, vertical currents, and the NLIW. Do sharks change their depth distribution in response to the NLIW? If sharks respond to the NLIW, do they move up and down passively with the wave vertical currents, or do they respond actively?

Methods

Trains of NLIW approaching the Southwest flank of Stellwagen Bank were measured on 23 July 2010 and 1 July 2011 from the anchored R/V Auk, in ~55 m water depth (Figure 1). Concurrently, large numbers of sharks were observed with acoustic backscatter for a total of 527 acoustic traces on July 1, and 3,240 on July 23. Boat position changed during the day, pivoting around the anchor with the tidal currents; the semidiurnal tide in the field site has a maximum range of ~3.1 m. These observations were taken while testing the hypothesis that humpback

whales aggregate in response to zooplankton and fish aggregation by predicable NLIW (Pineda et al. 2015).

The July 23 event featured small amplitude waves propagating over a perturbed field, and some waves appear superimposed. The July 1 event included clearly defined, large-amplitude waves propagating over a mostly unperturbed thermocline. Our analysis focused on the July 1 event, when we estimated wave phase speed and direction of propagation from Doppler profiler data, and derived vertical currents associated with individual shark traces. For the July 23 event, we present only shark distribution data.

Physical measurements

Current velocity, temperature, acoustic backscatter, and density. East, north and vertical current velocities were measured with a Doppler current meter. The 600 kHz RDI ADCP (4 transducers and beam angle 20°) sampled from the vessel looking-down every ping (1.4 s), and bin height was 1.5 m. Propagation direction φ and phase speed c of the NLIW on 1 July were estimated by solving the "antenna" problem (e.g., Ufford 1947; Lee 1961). The timing of the four leading depressions observed with ADCP's acoustic backscatter at a selected depth (~27 m) was noted for each beam, and time lags among beam-pairs were calculated for each wave depression. Lags among beam pairs in the four wave depressions were then averaged for the appropriate beam-pair. Derivation φ and c considered the mean heading of the instrument during the event and magnetic declination. Phase speed, c, was used to derive along-wave distance from time.

Acoustic backscatter was also measured with a Biosonics DTX echosounder (200 and 120 kHz transducers). The horizontal currents in the direction of internal wave propagation were obtained by rotating the east-north currents according to the propagation direction φ (e.g., Scotti et al. 2005). Beam spread in the ADCP results in sampling heterogeneous currents fields, and may lead to inaccurate horizontal velocity estimates. Further, averaging of the current field by the 4 beams likely smooths horizontal current velocities. The ADCP was programmed to produce horizontal earth coordinates (north south and east-west). Thus, the data cannot be corrected for beam spread using techniques that require beam coordinate data. Horizontal currents were only used to provide a visualization of the flow field in the July 1 event. The ADCP vertical currents were evaluated against independent estimates of vertical velocity derived from the Biosonics echosounder acoustic backscatter. Acoustic backscatter patterns from the echosounder were measured in the vicinity of the shark traces (within 10 m above and below), and vertical displacement of backscatter patterns with time was estimated (see Figure S1 legend for details). Temperature loggers (RBR 1060), attached on a line that was suspended from a large float, measured temperature every 10 s at depths ranging from 0.6 to 51.7 m. The float was tethered to the boat, and the line was kept taut by suspended weights. Logger spacing was 2.25 m on July 1, with shorter separation near the surface and bottom; spacing was 4.5 m on July 23. On July 1, three temperature loggers did not record data. Onboard the R/V AUK, the acoustic backscatter transducer and the Doppler current meter were ~5.5 m apart, whereas the temperature line was separated up to 30 m from the boat. On July 1, temperature was advanced to match the NLIW in

the acoustic backscatter and current meter data, and on July 23, temperature was retarded to match backscatter. Conductivity, temperature and depth profiles were taken with an RBR XR-620 CTD from downcast measurements, and density was derived from conductivity and temperature for the July 1 event.

Shark observations

Squalus acanthias is the most abundant coastal shark in the region (Bigelow and Schroeder 2002). Acoustic backscatter measurements were used to estimate shark depth and depth-change with time. The 200 and 120 kHz transducers were held ca. 1 m below the sea-surface and sampled at a rate of 5 pings per second. Only the 200 kHz transducer was used on 1 July, and most measurements on 23 July used the 200 kHz frequency, but 120 kHz data was used to resolve ambiguous data. The real-time acoustic data was used in conjunction with a live-feed cabled video camera (SplashCam Deep Blue Pro) to identify the backscatter traces characteristic of the sharks, with lighting provided by two small scuba LED flashlights. Traces of *S. acanthias* had characteristic 'rectangular' appearance, were between -50 db and 0 db, and easily distinguishable in the echograms (Figure 2 b). Traces that were less than 4.5 s in duration were not considered in the analysis. In cases where two traces occurred consecutively, each trace was assumed to represent a shark unless there were faint or broken traces between the two. Faint traces that were perfectly parallel to a shallower trace were assumed to be an echo reflection and disregarded. Shark traces that were within 1 – 1.5 m of the camera were also disregarded, in case

the lights influenced a shark's vertical position. We assumed individual traces were unique individual observations, but we likely measured some individuals more than once.

For each shark trace, depth Z, taken as the vertical middle of the trace, and ping number, an index of time T, were measured at the beginning (Z_1 , T_1), and end of trace (Z_2 ,T_2). These measurements were used to estimate depth-change rate for individual traces, DS:

$$DS = \frac{Z_2 - Z_1}{T_2 - T_1}$$

Depth of horizontal mid-point of the trace Z_{md} was also recorded. Vertical currents corresponding to each acoustic trace measurement (w_i) were obtained, and an average of the vertical currents ($\overline{w_i}$) were computed for the duration of each shark trace. Individual traces were difficult to differentiate at very high densities of *Squalus acanthias*, which often occurred on 23 July. At very high densities, measurements of *S. acanthias* traces were taken from sections of full length traces at any point where the trace was sufficiently distinct. Ping number and depth of a trace section was measured at the earliest point where the trace could be distinguished and before it merged into other traces. Finally, to describe the depth distribution of the shark aggregation, we calculated a 10-point running mean of shark depths, and we refer to this quantity as the mean-depth of the aggregation.

To resolve whether the July 1 NLIW vertical currents related to depth-change rate DS, we parsed the shark observations among those that occur in the steepest sections of the NLIW train, and all others. The steep sections were associated with the five leading depressions, and occurred

between 15:23 and 16:01 (see below), but some records within this interval were determined to occur in the non-steep section (e.g., around the waves crests and troughs, at times 15:29, 15:37, 15:37, 15:45, and 15:54). The steepest section of the NLIW were determined from wave patterns in ADCP acoustic backscatter (average of 4 beams for each wave depression), and the record was divided in sections with steep and non-steep patterns. The steepest sections corresponded to those where change in backscatter isopleth-depth with time dz/dt were $> |1.2|$ cm s^{-1}, at about 20 to 32 m water depth. (For comparison, dt/dz in the steepest sections at 20 - 32 m depth were up to dz/dt = 6 - 8 cm s^{-1}, and higher velocities at shallower depths).

Results

On 1 July, density stratification preceding the NLIW extended to surface waters (Figure 3). There were 5 clearly defined wave troughs with periods of ca. 8 minutes and amplitudes of up to 20 m, comprising about 2/5 of the water column (Figure 4). These waves are highly nonlinear with the nonlinearity parameter, the ratio of wave amplitude to upper layer depth, greater than one (Stanton and Ostrovsky 1998; Helfrich and Melville 2006). The well-defined waves had similar amplitude and period, and were followed by a set of irregular, smaller amplitude nonlinear internal waves. The estimated phase speed was c = 0.30 m s^{-1}, yielding a wavelength on the order of 150 m.

Some horizontal velocities in the direction of wave propagation u at 10-20 m were of similar magnitude to c (Figure 5), suggestive of trapped cores (Helfrich and White 2010; Luzzatto-Fegiz

and Helfrich 2014) and finite transport in the direction of wave propagation. These horizontal currents should be interpreted cautiously, however, because of biases in velocity estimates associated with beam spreading as mentioned earlier. The correlation between the ADCP vertical velocities, and acoustic backscatter estimates of vertical velocity was 0.83 (n=185) (Fig. S1), suggesting these two independent estimates of vertical velocity are consistent. The surface manifestation of the waves included bands of small breaking waves that rocked the boat as they passed by (Figure S22). Acoustic backscatter measurements during the event yielded 527 shark traces, identified as *Squalus acanthias* with the help of live video (Figure 2 a), with 185 traces in the steepest sections of the NLIW, and 342 in non-steep regions.

Shark distribution on 1 July centered around 20 m water depth at the beginning of the observations, about 14:00 UTC (10 AM local time, EST), with no sharks observed deeper than about 30 m (Figure 6). Mean-depth switched at about 14:45, when sharks were at 30 to 40 m depths, with only a few individuals observed around 20 m. Sharks moved deeper in response to the NLIW just past 15:20, with no sharks in shallow water. The mean-depth of the aggregation appeared to move up and down with the isotherms during the first five depressions, and the deepest distributions in 1 July were associated with the second and fourth depressions (Figure 6). Few sharks were observed from 16:30 to about 17:00, and the distribution observed thereafter was broad, with sharks from ca. 15 to 50 m depth.

Wave amplitude was smaller and sharks were more abundant on the 23 July event (number of shark traces = 3,240). During the first two and largest depressions, shark mean-depth moved up

and down with the waves. The mean-depth, estimated as the 10-point running mean, fluctuated around 35 m (Figure 7). Sharks were very abundant between 15:00 and 15:30, and between 15:15 and 15:20, a large number were in shallow 10-20 m waters. The depth range of the distribution tended to be large, although a relatively small number of sharks were observed in waters shallower than 20 m from approximately the beginning of the largest waves, just past 13:30 to ca. 15:01. Inspection of the echograms indicate that on 23 July the distribution was sometimes bi-modal, with a group of individuals near the bottom, and another group at 35 or 25 m water depth.

DS in the steep portions of the NLIW train tended to correlate positively with the mean vertical currents, indicating that individual shark traces move up and down with the ascending and descending currents (Figure 8 a). However, no pattern was observed for the sharks in the non-steep portion of the NLIW (Figure 8 b). The patterns in the steep portion of the NLIW may relate to a passive response, where sharks move up and down in concert with the vertical currents, or an active one, where individuals may swim up or down in response to the NLIW. To resolve whether *DS* may have changed with the sign and magnitude of the vertical currents, average vertical currents $\overline{w_i}$ were subtracted from *DS* for each observation and plotted as a function of $\overline{w_i}$. The trend in $DS - \overline{w_i}$ as a function of $\overline{w_i}$ was characterized with a cubic polynomial, and a 10-point running mean. If sharks behave as passive particles, such a plot should show no trend. For the negative, downward currents, patterns suggest no response, that is, sharks appear to move down with similar velocities than those associated with the sinking thermocline (Figure 9). For

the positive, upward currents, however, the trend indicates a slight increase at velocities 0.06 m s^{-1}, and a more pronounced decrease at velocities larger than 0.08 m s^{-1}, suggesting that sharks swam down at the highest positive currents (Figure 9).

We tested whether the patterns described above were due to chance with a randomization analysis (Manly 1997). First, we calculated the sum of the squared residuals from fitting the polynomial cubic model to the $\overline{w_i}$ vs. ($DS - \overline{w_i}$) data (e.g., Figure 9). Then, we randomly reassigned ($DS - \overline{w_i}$) values to the $\overline{w_i}$ data, fit a cubic polynomial, calculated the sum of squared residuals, and repeated 100,000 times (Figure 10). The approximate *p* is the proportion of sum of squared residuals from the randomizations that are smaller than the sum of squared residuals derived from the non-randomized data set (1.1685, p=0.00005). These results suggest the trends described by the cubic polynomial fit are not random.

Discussion

Our study adds to the diversity of NLIW observed in Massachusetts Bay, including rank-ordered undular bores (Haury et al. 1979; Butman et al. 2006) and waves of elevation (Scotti and Pineda 2004). In particular, the 1 July event is remarkable as the set of clearly defined waves had comparable period and amplitude –e.g., not a rank-order wave train, had a vivid surface expression, and O(1) non-linearity. The current velocity and temperature measurements, with sharp horizontal temperature gradients near the surface, suggest mass transport in the direction of wave propagation. Density stratification extended to the surface, and mass transport in trapped

cores can occur in these conditions (Helfrich and White 2010). Studies in this region have identified two local generation sites: Stellwagen Bank (e.g. Haury et al. 1979), and Race Point channel (da Silva and Helfrich 2008). The NLIW on 1 and 23 July likely originated off Race Point, as do the majority of NLIW observed in the southwest flank of Stellwagen Bank (Pineda et al. 2015). Moreover, the observation of superimposed NLIW trains is consistent with generation of two NLIW sets at Race Point (da Silva and Helfrich 2008).

Nonlinear internal waves are ubiquitous in the world ocean. Yet, their unpredictability and small temporal scales, coupled with the difficulty in resolving the biological response, has hindered understanding on how NLIW influence the behavior and distribution of pelagic organisms, from microbes to whales. The response of organisms to NLIW and other processes where vertical currents are significant can be passive or active. Further, their effects on distribution, or organism's physiological and ecological condition, can be direct, where currents and turbulence, or the interaction of these with individual behavior, produces changes in distribution (or individual condition) or indirect, where a variable forced by the waves results in a change in distribution or condition (Table 1). Temporal and spatial changes in horizontal distribution that parallel pycnocline deformation caused by the NLIW suggest a passive response (e.g., Haury et al. 1983). An active behavioral response with a direct influence on distribution may result from plankton swimming up against downwelling currents, resulting in accumulation and transport in internal tidal bore warm fronts (Pineda 1999). NLIW might also change indirectly the depth distribution of pelagic organisms, as when thinning and thickening of the surface turbid layer by

NLIW changes the light environment at depth, resulting in short-term vertical migrations of fish (Kaartvedt et al. 2012).

Observing plankton and nekton active response to vertical currents in the field is challenging. Thus, observational studies have used indirect approaches, whereby behavior is inferred from pelagic distribution patterns and assumed or measured vertical currents (e.g., Pineda 1999; Lennert-Cody and Franks 2002). Laboratory studies can more easily resolve both circulation and behavior (e.g., DiBacco et al. 2011). Our unique data set allowed us to measure the response of sharks to the 1 July NLIW event. Results indicate a range of responses, from passive to active, and that the changes in organism distribution were likely in direct response to the NLIW. There was no trend in $(DS - \overline{w_i})$ for downward currents, suggesting that sharks respond passively to the NLIW when the thermocline was sinking. At the highest velocities of the upward phase of the wave, however, sharks appear to respond actively by swimming down. These large-amplitude waves clearly influenced the short-term depth distribution of the sharks *Squalus acanthias.*

What are the consequences, and what might be the ultimate causes, explaining sharks swimming down during the fastest upward currents? The individual responses of the sharks might have influenced aggregation mean-depth. During the 1 July event, the center of mass of the distribution deepened during the NLIW event and approximately 90% of the shark traces were associated with waters < 10.2°C. During the 23 July event, with smaller amplitude waves, deepening in the distribution occurred during the first two depressions, although this depth

distribution appears similar to other times during that day. On 23 July, about 90% of sharks were in waters < 11.8°C. On 1 July, the deeper distribution resulting from NLIW exposed sharks to temperatures as cold as 6.2 °C, with metabolic consequences for the sharks (e.g., Brett and Blackburn 1978). The deeper distribution might have also exposed the sharks to a different prey field, with potential for bentho-pelagic coupling and community structure consequences. Strong NLIW-induced currents can extend to the bottom at this location (e.g., Pineda et al. 2015) and cause sediment resuspension (Butman et al. 2006), and this might intensify trophic interactions by, for example, resuspending chemical olfactory cues that may elicit a predatory response. The proximate and ultimate factors that caused sharks to response to the ascending thermocline are unknown, but by swimming down they might have escaped the horizontal shear associated with the upper water column. Thus, we speculate that sharks swam down in response to the upward fast currents to avoid areas of maximum shear.

This study characterized the response of *Squalus acanthias* to NLIW using high-frequency acoustic backscatter profiles. This enabled us to quantify shark distribution and behavior from hundreds of observations at temporal scales commensurate to NLIW variability. While shark (and other large nekton) spatial distribution and behavior can be measured by acoustic telemetry, and tagging studies have been used to measure top predator vertical movements in stratified waters (Eckert and Stewart 2001; Aspillaga et al. 2017), tagging approaches have a number of limitations, including physical interference with the animals, and number of individuals that can be tagged. In order to generate data comparable to that obtained in this study, a very large

number of individuals would need to be tagged to ensure a reasonable chance that those individuals were present at the time and location of NLIW. Furthermore, acoustic telemetry studies typically capture data at a lower sampling frequency than in our study, but for a longer time period (Hussey et al. 2015). Although backscatter data has limitations, including potential difficulties in differentiating traces and the need to identify the animals producing traces (e.g. through live-feed video camera), acoustic backscatter data to study fish behavior allows simultaneous measurement of a large number of individuals and is a non-invasive technique (Fielding et al. 2004; Colbo et al. 2014). Future studies that combine approaches (e.g. telemetry and acoustic backscatter data) could be used to understand how fine-scale behavioral responses translate into longer term, large-scale distribution patterns.

Understanding the full range of behavior and individual movements of *Squalus acanthias* has been identified as an urgent priority to aid the conservation and management of this globally declining species (Thorburn et al. 2018). Our results contribute to the growing body of research documenting how hydrodynamic processes influence marine vertebrate distributions (e.g., Yen et al. 2004; Hooker et al. 2011; Scales et al. 2014), and in particular show that high-frequency processes are useful in understanding the vertical component of large nekton distribution. While large aggregations of sharks were observed at Stellwagen Bank during the two NLIW events, it is not known whether sharks regularly aggregate at this site in response to NLIW. If sharks do persistently aggregate at sites with NLIW or other high frequency processes, such areas may deserve special consideration for conservation activities. Additionally, understanding the

magnitude and predictability of associations between sharks and NLIW will aid efforts to characterize biological-physical coupling in marine ecosystems, and ultimately help predict habitat use for large apex predators (Yen et al. 2004).

Acknowledgements

Thanks to the personnel that helped us in the cruise and logistics, including Brad Cabe, Michael Thompson, and the crew of the R/V Auk. Andy Solow suggested to randomize the sum of square residuals. This work was supported by Woods Hole Sea Grant, and the Woods Hole Oceanographic Institution.

Tables

Table 1. Hypothetical examples of organism's responses (passive/active) to processes featuring vertical currents, and mode of influence in organism's distribution or physiological and ecological condition (indirect/direct).

	Passive	Active
Indirect	Sessile benthic organisms buried by sediments resuspended by NLIW.	Intensification of trophic interactions due to prey aggregation.
Direct	Changes in organism's depth distribution parallels pycnocline depth.	Organisms swim up in response to vertical displacement. Distribution can differ from that of a passive tracer.

Figure legends

Fig. 1. Detailed and wide-perspective maps of the study area. The arrow in the detailed map points in the estimated direction of propagation in the July 1 NLIW event, and arrow origin indicates the site of the observations at the southwest flank of Stellwagen Bank. The suspected generation site is near Race Point channel (da Silva and Helfrich 2008), about 10 km distant from the study site. Contour lines every 15 m. Digital bathymetry from Butman et al. (2007). Upper right corner is eastern United States and Canada. Stellwagen Bank is designated by the box near the horizontal arrow. Digital coastline from NOAA's National Geophysical Data Center.

Fig. 2. Sharks and first wave of depression on July 1. **(a)** Screen-capture photographs of *Squalus acanthias* from video camera. **(b)** Echogram with shark traces and an internal wave on July 1 (first wave of depression). Shark traces are bounded by white and yellow markers. The broken feature at ~1,850 and 2,400 pings and 26 m is the camera (red markers). The sharp feature at ca. 54 m is the bottom.

Fig. 3. Density (solid gray line) and temperature (dotted line) profiles at 13:42, before the NLIW. The CTD sampled the entire water column.

Fig. 4. Internal wave train from temperature, July 1. Along-wave distance was derived from time by using estimated phase speed *c*. Open symbols at ~ -160 m represent temperature loggers.

Fig. 5. First two depressions of the NLIW train measured with acoustic backscatter (Biosonics), 14 °C isotherm, and currents in the direction of propagation on July 1 (negative arrows are in the direction of propagation). Propagation speed was subtracted from the currents, and along-wave distance was derived from time by using estimated phase speed *c*. Therefore, currents are relative to estimated phase speed.

Fig. 6 Shark depth Z_{md} and 18, 14 and 10 °C isotherms on July 1.

Fig. 7 Shark depth Z_{md} and 20, 18, 14 and 10 °C isotherms on July 23.

Fig. 8 Depth-change rate (*DS*) as a function of mean vertical currents , $\overline{w_i}$, on July 1. Individuals in **(a)** the steep regions and **(b)** non-steep regions of the NLIW.

Fig. 9. DS with mean vertical currents $\overline{w_i}$ removed as a function of $\overline{w_i}$, for traces in the steep section of the NLIW, 10-point running mean (dotted line), and cubic polynomial fit (solid line).

Fig. 10. Frequency distribution of the sum squared residuals (ssr) from cubic polynomial fit of 100,000 randomized DS - $\overline{w_i}$ values. The ssr from the observed data and approximate p are also given.

References

Aspillaga, E., F. Bartumeus, R. M. Starr, À. López-Sanz, C. Linares, D. Díaz, J. Garrabou, M. Zabala, and B. Hereu. 2017. Thermal stratification drives movement of a coastal apex predator. Scientific reports **7:** 526.

Bigelow, A. F., and W. C. Schroeder [eds.]. 2002. Bigelow and Schroeder's Fishes of the Gulf of Maine, 3rd ed. Smithsonian Institution Press.

Brett, J., and J. Blackburn. 1978. Metabolic rate and energy expenditure of the spiny dogfish, *Squalus acanthias*. Journal of the Fisheries Board of Canada **35:** 816-821.

Butman, B., P. S. Alexander, A. Scotti, R. C. Beardsley, and S. P. Anderson. 2006. Large internal waves in Massachusetts Bay transport sediments offshore. Cont. Shelf Res. **26:** 2029-2049.

Butman, B., P. C. Valentine, T. J. Middleton, and W. W. Danforth. 2007. A GIS Library of multibeam data for Massachusetts Bay and the Stellwagen Bank National Marine Sanctuary, Offshore of Boston, Massachusetts. U.S. Geological Survey Data Series 99, DVD-ROM. Available online at http://pubs.usgs.gov/ds/99/.

Colbo, K., T. Ross, C. Brown, and T. Weber. 2014. A review of oceanographic applications of water column data from multibeam echosounders. Estuar. Coast. Shelf Sci. **145:** 41-56.

Cortés, E., F. Arocha, L. Beerkircher, F. Carvalho, A. Domingo, M. Heupel, H. Holtzhausen, M. N. Santos, M. Ribera, and C. Simpfendorfer. 2010. Ecological risk assessment of pelagic sharks caught in Atlantic pelagic longline fisheries. Aquatic Living Resources **23:** 25-34.

da Silva, J. C. B., and K. R. Helfrich. 2008. Synthetic Aperture Radar observations of resonantly generated internal solitary waves at Race Point Channel (Cape Cod). J. Geophys. Res. - Oceans **113:** C11016.

DiBacco, C., H. Fuchs, J. Pineda, and K. Helfrich. 2011. Swimming behavior and velocities of barnacle cyprids in a downwelling flume. Mar. Ecol. Prog. Ser. **433:** 131-148.

Eckert, S. A., and B. S. Stewart. 2001. Telemetry and satellite tracking of whale sharks, *Rhincodon typus*, in the Sea of Cortez, Mexico, and the north Pacific Ocean, p. 299-308. The behavior and sensory biology of elasmobranch fishes: an anthology in memory of Donald Richard Nelson. Springer.

Fielding, S., G. Griffiths, and H. Roe. 2004. The biological validation of ADCP acoustic backscatter through direct comparison with net samples and model predictions based on acoustic-scattering models. ICES. J. Mar. Sci. **61:** 184-200.

Fordham, S., S. Fowler, R. Coelho, K. Goldman, and M. Francis. 2006. *Squalus acanthias*. The IUCN Red List of Threatened Species 2016: e. T91209505A2898271. Gland, Switzerland: International Union for Conservation of Nature.

Greer, A. T., R. K. Cowen, C. M. Guigand, J. A. Hare, and D. Tang. 2014. The role of internal waves in larval fish interactions with potential predators and prey. Prog. Oceanogr. **127:** 47-61.

Haury, L. R., M. B. Briscoe , and M. H. Orr. 1979. Tidally generated internal wave packets in Massachusetts Bay. Nature **278:** 312-317.

Haury, L. R., P. H. Wiebe, M. H. Orr, and M. G. Briscoe. 1983. Tidally generated high-frequency wave packets and their effect on plankton in Massachusetts Bay. J. Mar. Res. **41:** 65-112.

Helfrich, K. R., and W. K. Melville. 2006. Long nonlinear internal waves. Annual Review of Fluid Mechanics **38:** 395-425.

Helfrich, K. R., and B. L. White. 2010. A model for large-amplitude internal solitary waves with trapped cores. Nonlin. Proc. Geophys. **17:** 303-318.

Hooker, S. K., A. Cañadas, K. D. Hyrenbach, C. Corrigan, J. J. Polovina, and R. R. Reeves. 2011. Making protected area networks effective for marine top predators. Endangered Species Research **13:** 203-218.

Hussey, N. E., S. T. Kessel, K. Aarestrup, S. J. Cooke, P. D. Cowley, A. T. Fisk, R. G. Harcourt, K. N. Holland, S. J. Iverson, and J. F. Kocik. 2015. Aquatic animal telemetry: a panoramic window into the underwater world. Science **348:** 1255642.

Jensen, A. C. 1965. Life history of the the spiny dogfish. Fishery Bulletin **65:** 527-553.

Kaartvedt, S., T. Klevjer, and D. Aksnes. 2012. Internal wave-mediated shading causes frequent vertical migrations in fishes. Mar. Ecol. Prog. Ser. **452:** 1-10.

Lee, O. S. 1961. Observations on internal waves in shallow water. Limnol. Oceanogr. **6:** 312-321.

Leichter, J. J., H. L. Stewart, and S. L. Miller. 2003. Episodic nutrient transport to Florida coral reefs. Limnol. Oceanogr. **48:** 1394–1407.

Lennert-Cody, C., and P. J. S. Franks. 2002. Fluorescence patches in high-frequency internal waves. Mar. Ecol. Prog. Ser. **235:** 29-42.

Link, J. S., L. P. Garrison, and F. P. Almeida. 2002. Ecological interactions between elasmobranchs and groundfish species on the northeastern US continental shelf. I. Evaluating predation. North American Journal of Fisheries Management **22:** 550-562.

Luzzatto-Fegiz, P., and K. R. Helfrich. 2014. Laboratory experiments and simulations for solitary internal waves with trapped cores. J. Fluid Mech. **757:** 354-380.

Manly, B. 1997. Randomization, bootstrap and Monte Carlo methods in biology, 2nd ed. CRC Press.

Nammack, M. F., J. Musick, and J. Colvocoresses. 1985. Life history of spiny dogfish off the northeastern United States. Trans. Am. Fish. Soc. **114:** 367-376.

Pineda, J. 1999. Circulation and larval distribution in internal tidal bore warm fronts. Limnol. Oceanogr. **44:** 1400-1414.

Pineda, J., V. Starczak, J. C. B. Da Silva, K. Helfrich, M. Thompson, and D. Wiley. 2015. Whales and waves: Humpback whale foraging response and the shoaling of internal waves at Stellwagen Bank. J. Geophys. Res. Oceans **120**.

Scales, K. L., P. I. Miller, L. A. Hawkes, S. N. Ingram, D. W. Sims, and S. C. Votier. 2014. On the Front Line: frontal zones as priority at-sea conservation areas for mobile marine vertebrates. J. Appl. Ecol. **51:** 1575-1583.

Scotti, A., B. Butman, R. C. Beardsley, P. S. Alexander, and S. Anderson. 2005. A modified beam-to-earth transformation to measure short-wavelength internal waves with an acoustic Doppler current profiler. Journal of Atmospheric and Oceanic Technology **22:** 583-591.

Scotti, A., and J. Pineda. 2004. Observation of very large and steep internal waves of elevation near the Massachusetts coast. Geoph. Res. Let. **31:** L22307.

Shepherd, T., F. Page, and B. Macdonald. 2002. Length and sex-specific associations between spiny dogfish (*Squalus acanthias*) and hydrographic variables in the Bay of Fundy and Scotian Shelf. Fish Oceanogr **11:** 78-89.

Sims, D. W., E. J. Southall, G. A. Tarling, and J. D. Metcalfe. 2005. Habitat-specific normal and reverse diel vertical migration in the plankton-feeding basking shark. J. Anim. Ecol. **74:** 755-761.

Stanton, T. P., and L. A. Ostrovsky. 1998. Observations of highly nonlinear internal solitons over the continental shelf. Geoph. Res. Let. **25:** 2695-2698.

Stehlik, L. L. 2007. Spiny dogfish, Squalus acanthias, life history and habitat characteristics, p. 44. NOAA Technical Memorandum NMFS-NE-203. NOAA.

Sulikowski, J. A., B. Galuardi, W. Bubley, N. B. Furey, W. B. Driggers III, G. W. Ingram Jr, and P. C. Tsang. 2010. Use of satellite tags to reveal the movements of spiny dogfish *Squalus acanthias* in the western North Atlantic Ocean. Mar. Ecol. Prog. Ser. **418:** 249-254.

Thorburn, J., R. Jones, F. Neat, C. Pinto, V. Bendall, S. Hetherington, D. M. Bailey, N. Leslie, and C. Jones. 2018. Spatial versus temporal structure: Implications of inter-haul variation and relatedness in the North-east Atlantic spurdog *Squalus acanthias*. Aquatic Conservation: Marine and Freshwater Ecosystems **28:** 1167-1180.

U.S. Department of Commerce. 2010. Stellwagen Bank National Marine Sanctuary Final Management Plan and Environmental Assessment. U.S. Department of Commerce, National Oceanic and Atmospheric Administration, Office of National Marine Sanctuaries.

Ufford, C. W. 1947. Internal waves measured at three stations. Transactions, American Geophysical Union **28:** 87-95.

Vianna, G. M., M. G. Meekan, J. J. Meeuwig, and C. W. Speed. 2013. Environmental influences on patterns of vertical movement and site fidelity of grey reef sharks (*Carcharhinus amblyrhynchos*) at aggregation sites. PLoS One **8:** e60331.

Yen, P. P., W. J. Sydeman, and K. D. Hyrenbach. 2004. Marine bird and cetacean associations with bathymetric habitats and shallow-water topographies: implications for trophic transfer and conservation. J. Mar. Sys. **50:** 79-99.

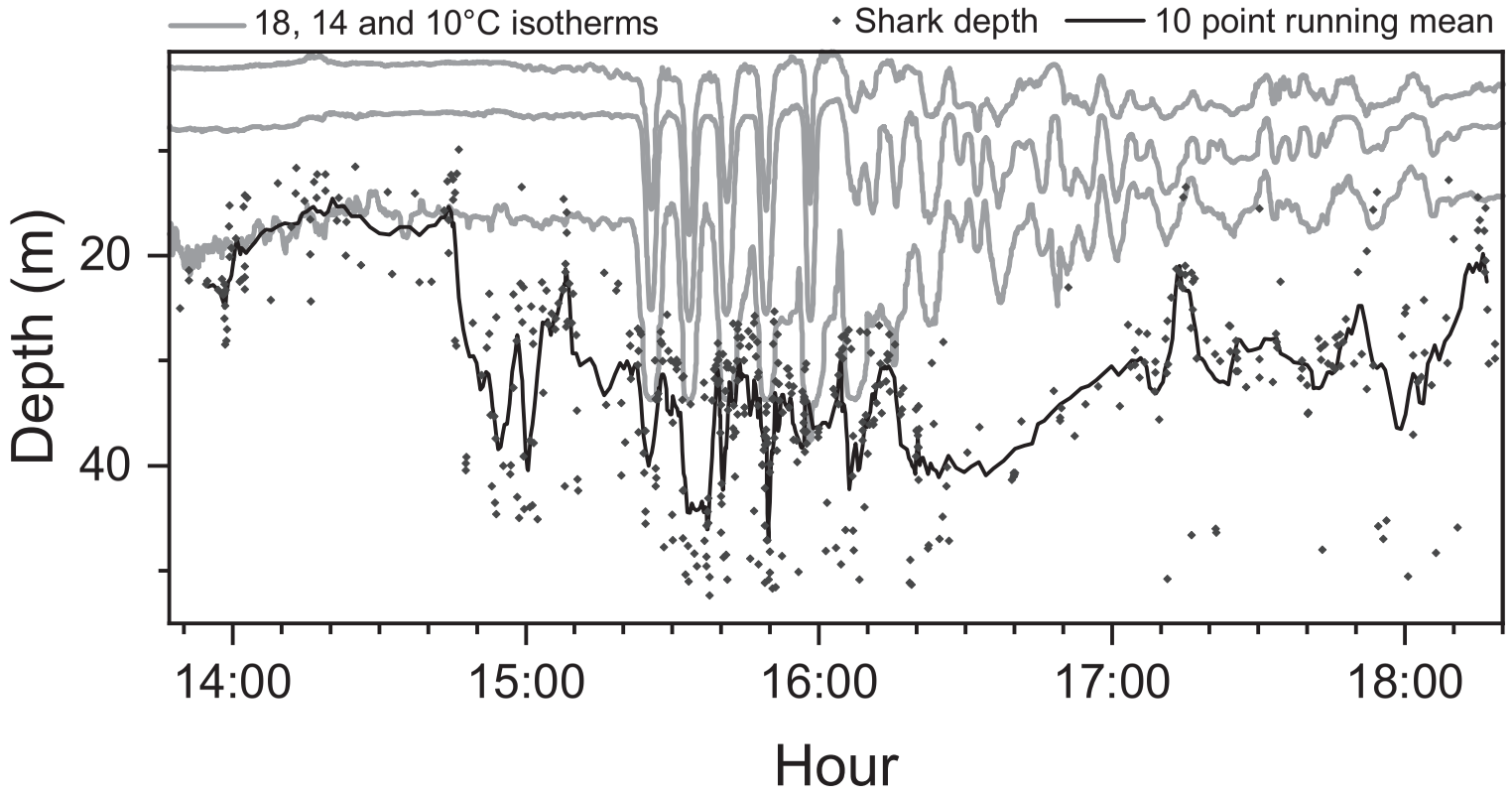

Fig. 6 Shark depth Zmd and 18, 14 and 10 °C isotherms on July 1.

Online version

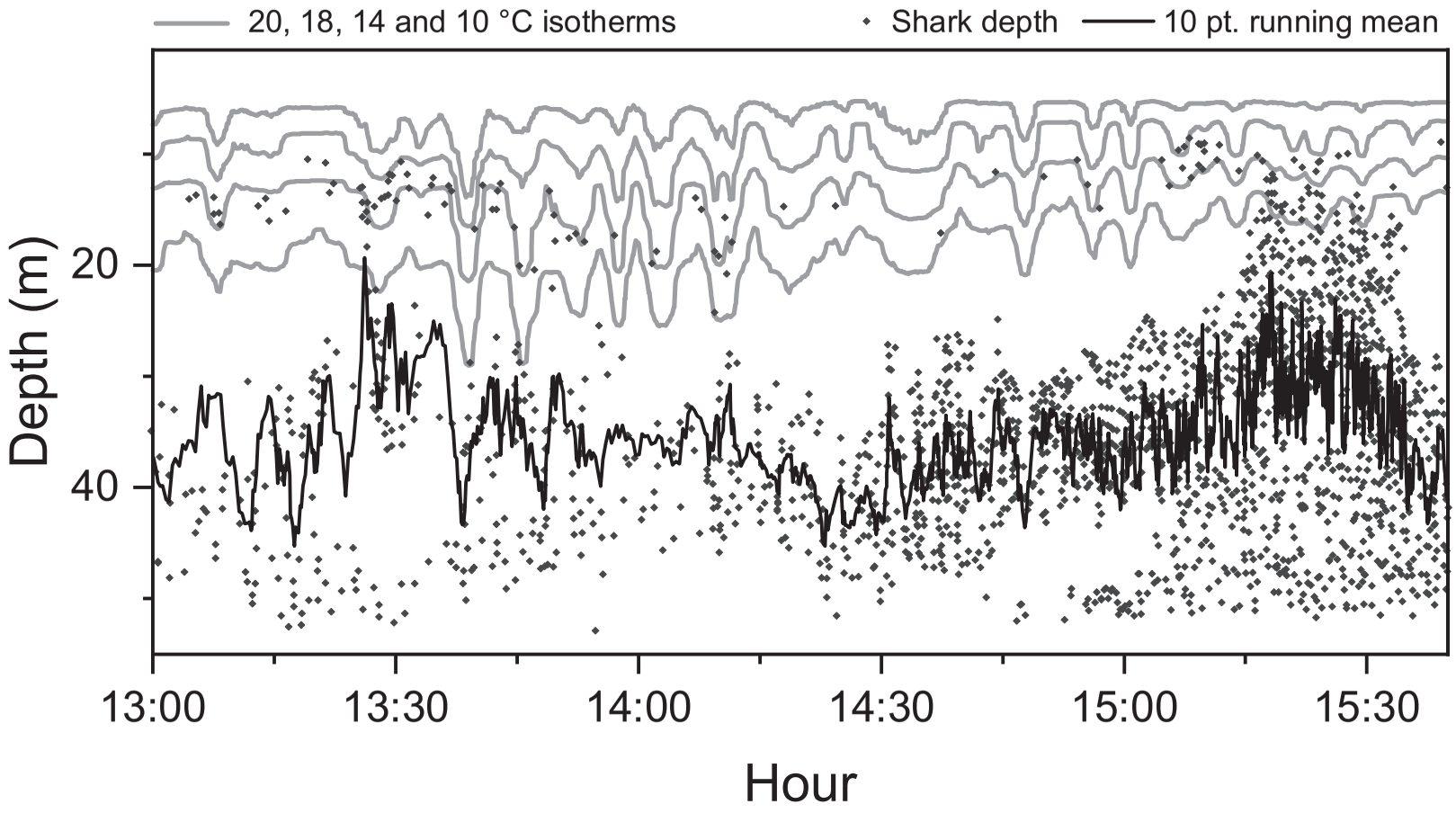

Fig.7 Shark depth Zmd and 20, 18, 14 and 10 °C isotherms on July 23

Online version

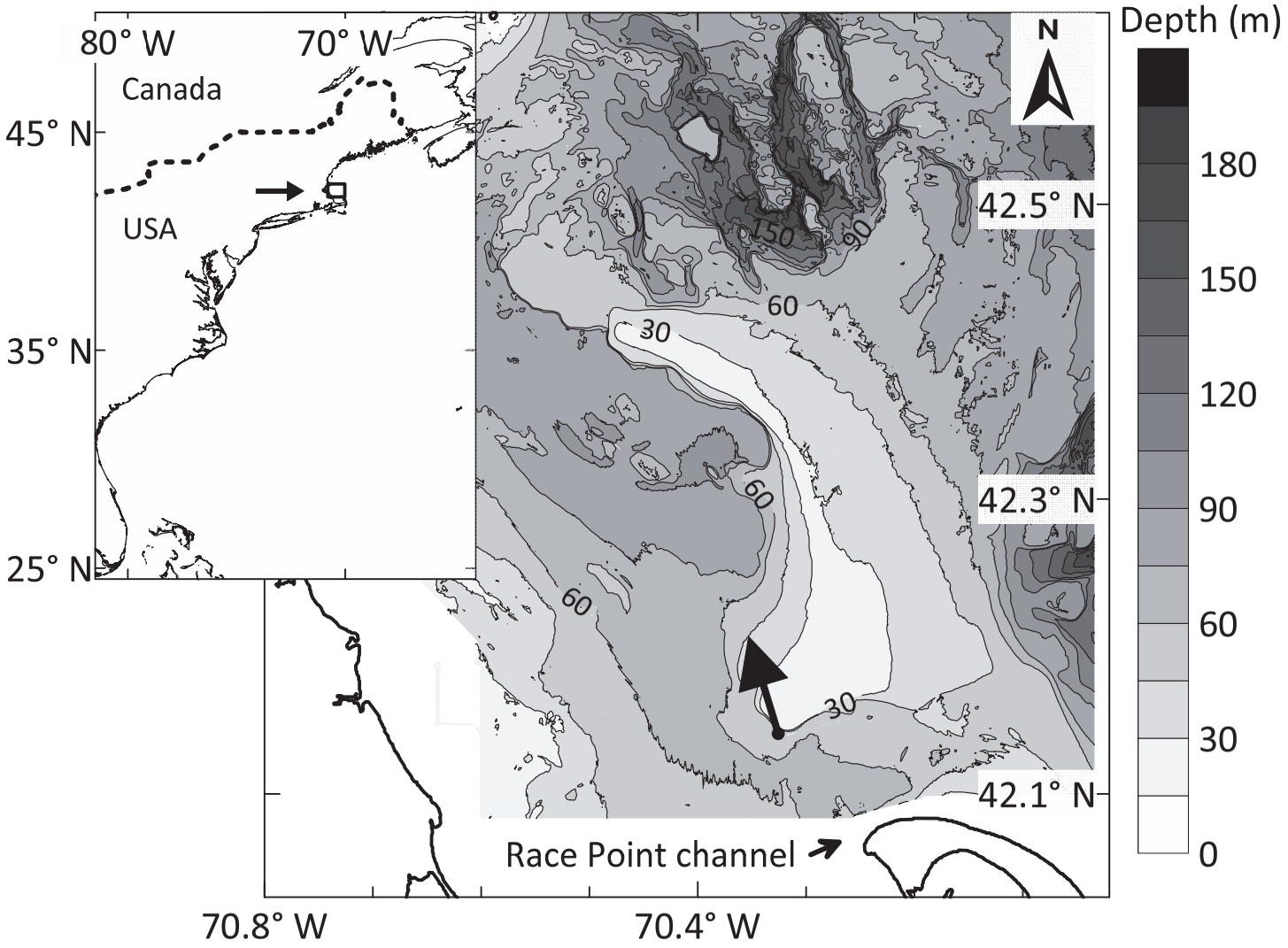

Fig. 1. Detailed and wide-perspective maps of the study area. The arrow in the detailed map points in the estimated direction of propagation in the July 1 NLIW event, and arrow origin indicates the site of the observations at the southwest flank of Stellwagen Bank. The suspected generation site is near Race Point channel (da Silva and Helfrich 2008), about 10 km distant from the study site. Contour lines every 15 m. Digital bathymetry from Butman et al. (2007). Upper right corner is eastern United States and Canada. Stellwagen Bank is designated by the box near the horizontal arrow. Digital coastline from NOAA's National Geophysical Data Center.

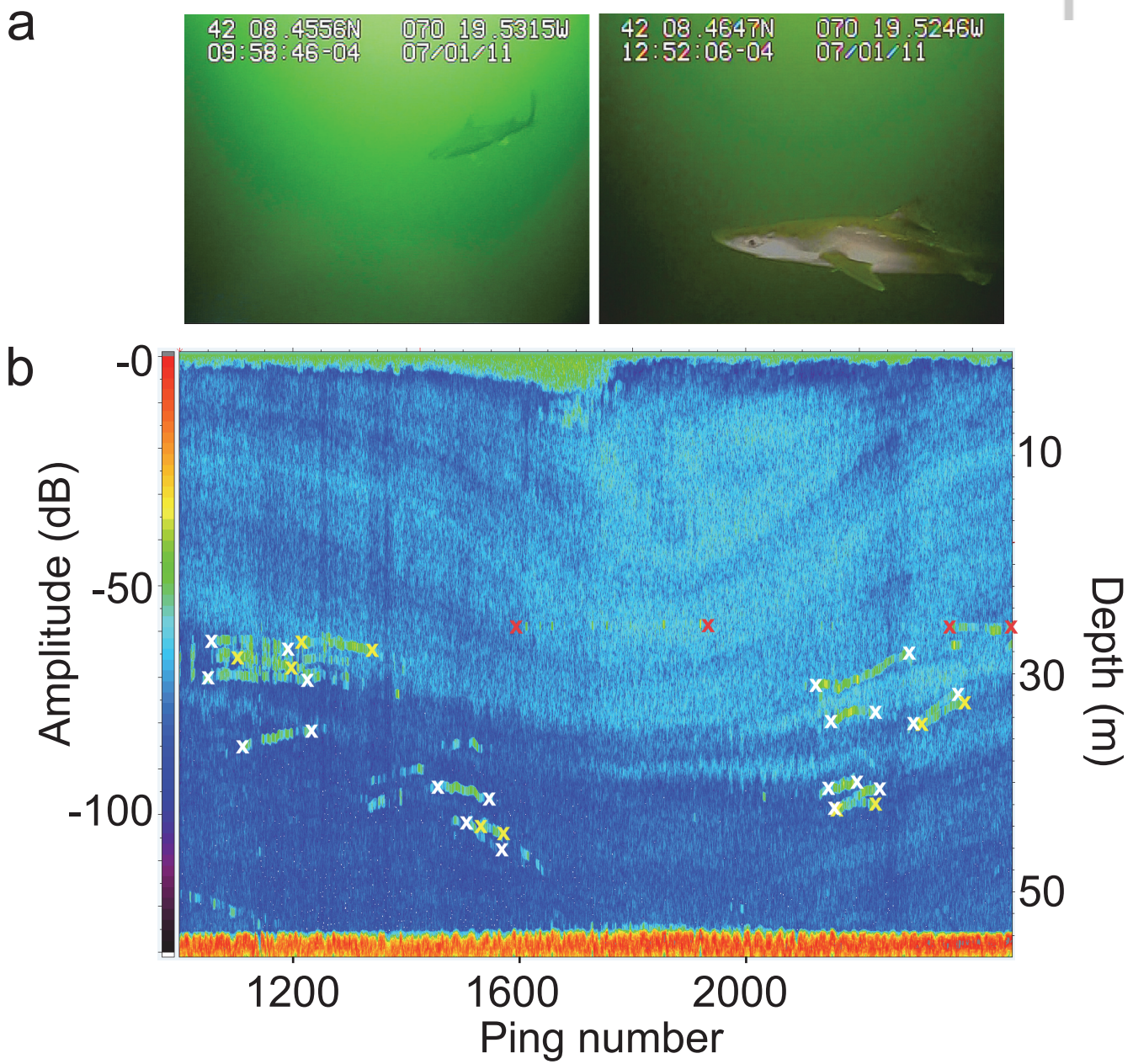

Fig. 2. Sharks and first wave of depression on July 1. (a) Screen-capture photographs of Squalus acanthias from video camera. (b) Echogram with shark traces and an internal wave on July 1 (first wave of depression). Shark traces are bounded by white and yellow markers. The broken features at ~1,850 and 2,400 pings and 26 m is the camera (red markers). The sharp feature at ca. 54 m is the bottom.

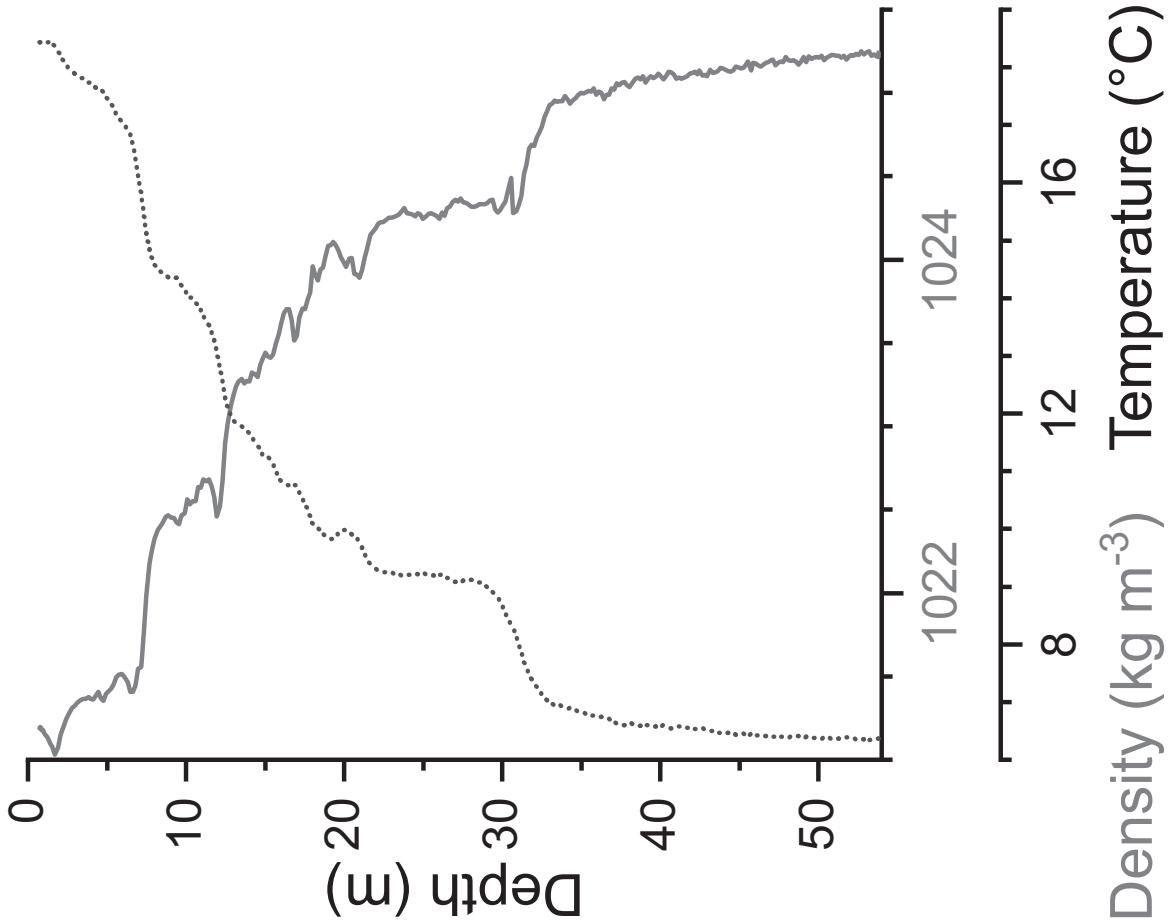

Fig. 3. Density (solid gray line) and temperature (dotted line) profiles at 13:42, before the NLIW. The CTD sampled the entire water column.

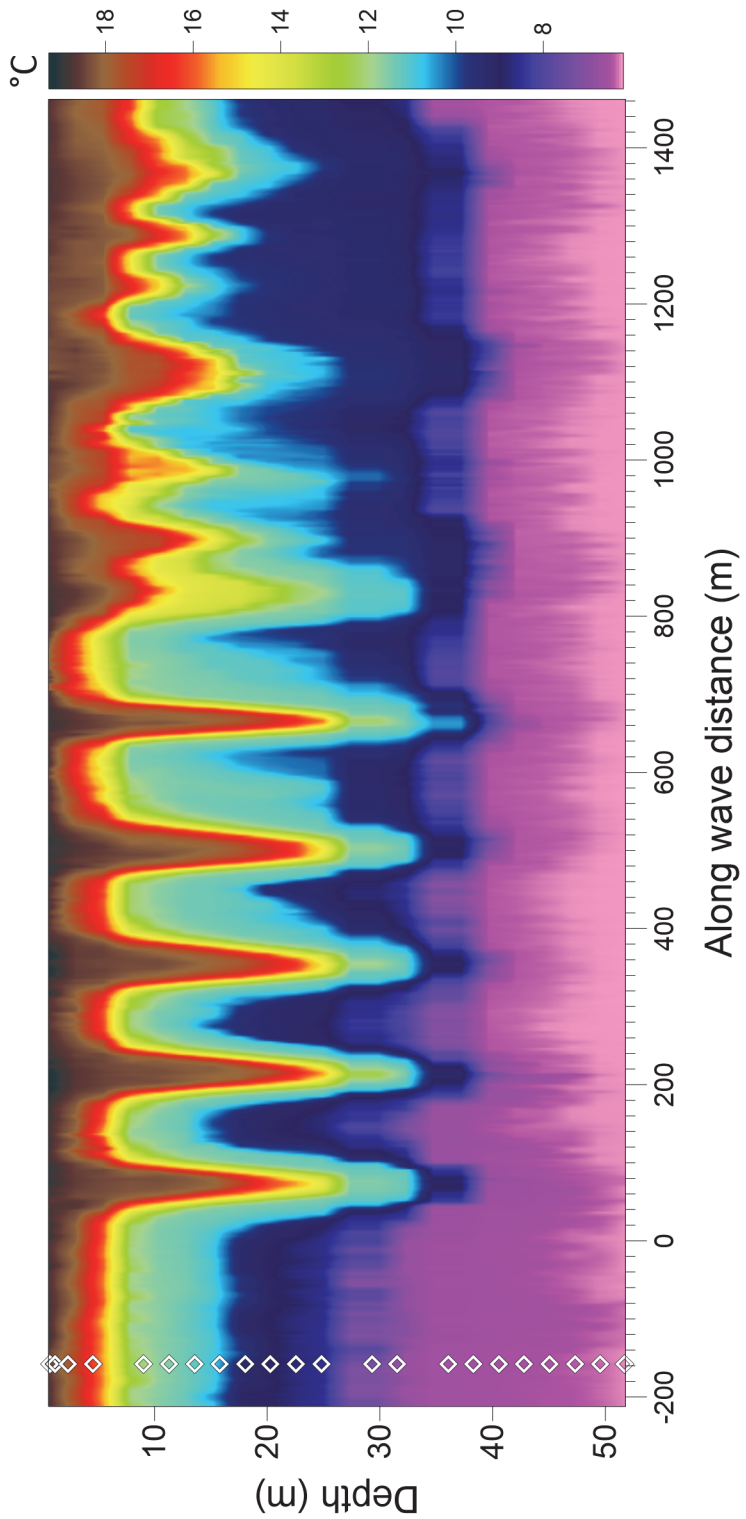

Fig. 4. Internal wave train from temperature July 1. Along-wave distance was derived from time by using estimated phase speed c. Open symbols at ~ -160 m represent temperature loggers.

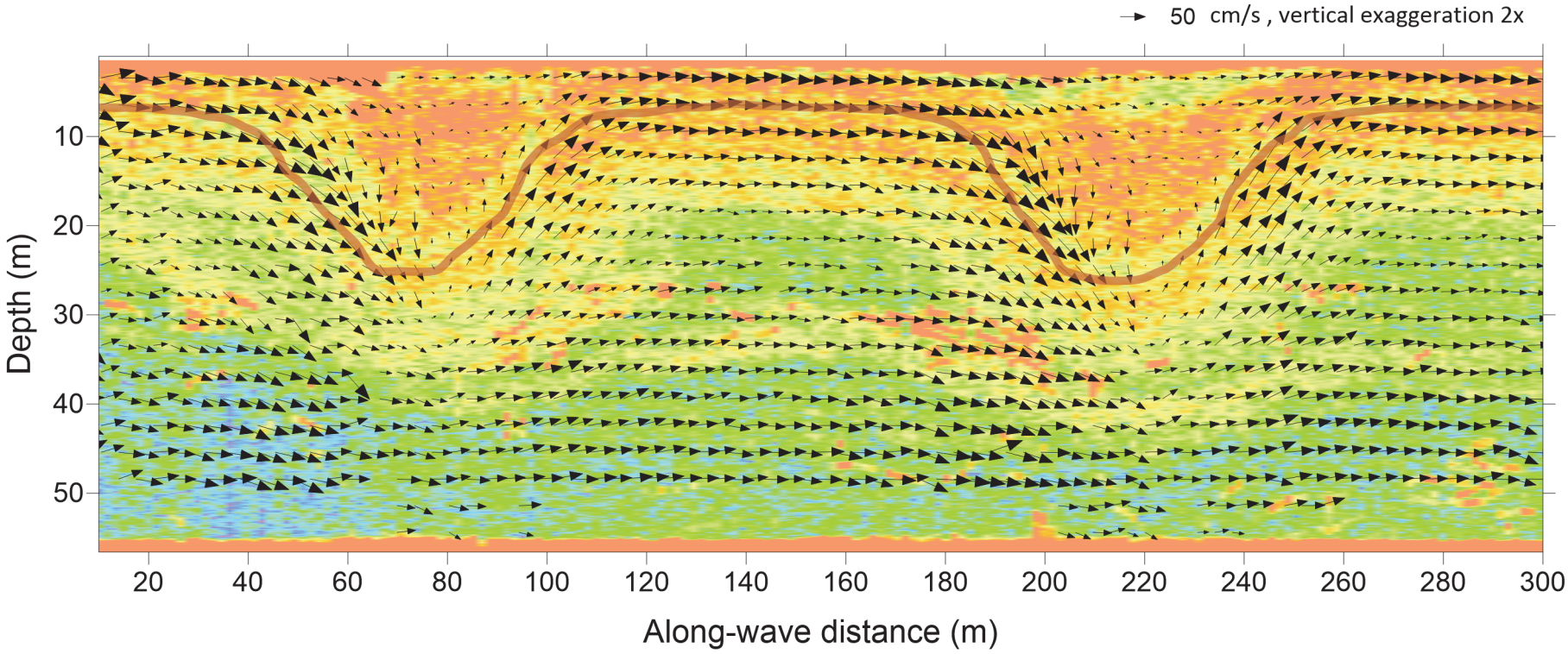

Fig. 5. First two depressions of the NLIW train measured with acoustic backscatter (Biosonics), 14 °C isotherm, and currents in the direction of propagation on July 1 (negative arrows are in the direction of propagation). Propagation speed was subtracted from the currents, and along-wave distance was derived from time by using estimated phase speed c. Therefore, currents are relative to estimated phase speed.

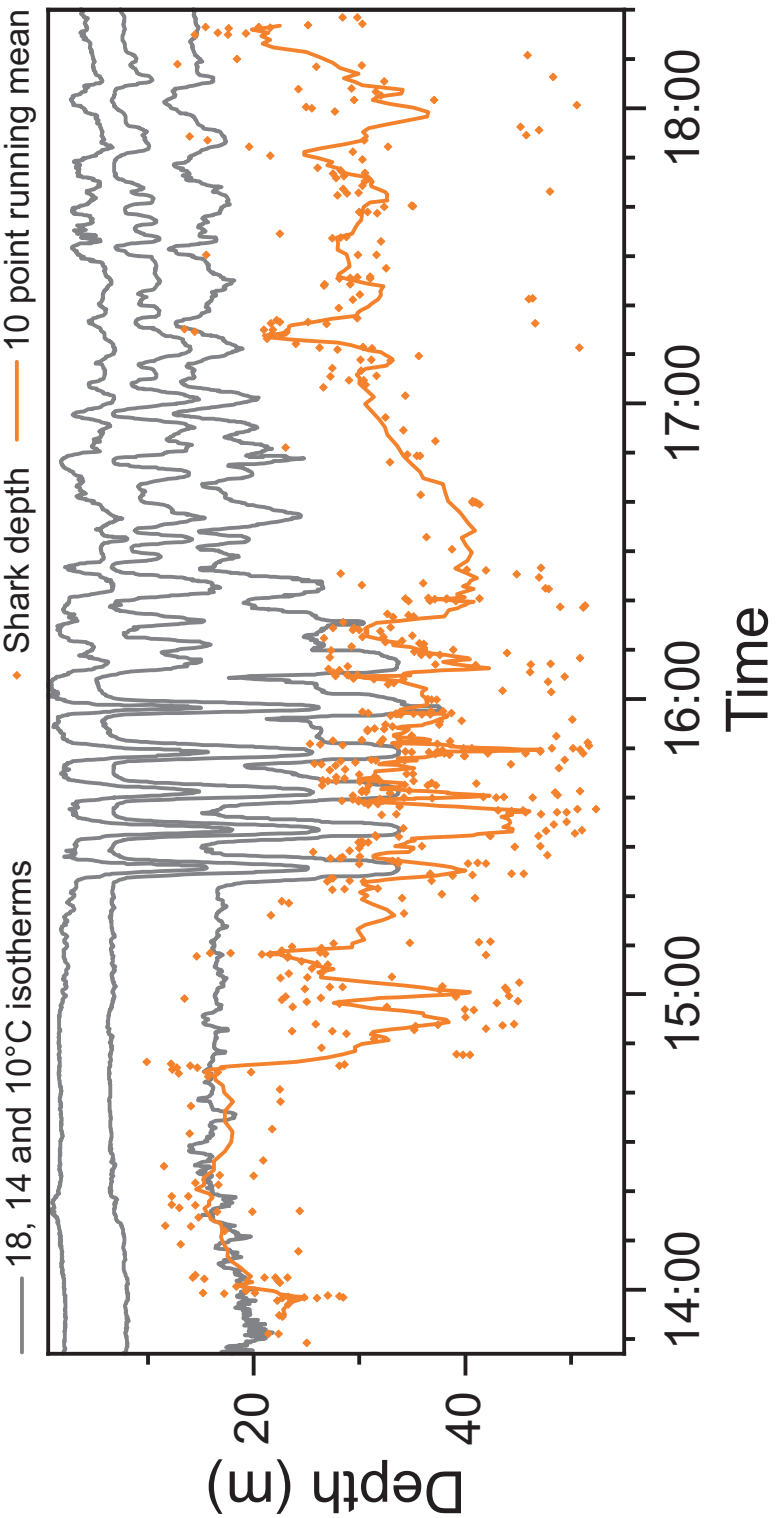

Fig. 6 Shark depth Zmd and 18, 14 and 10 °C isotherms on July 1.

Online version

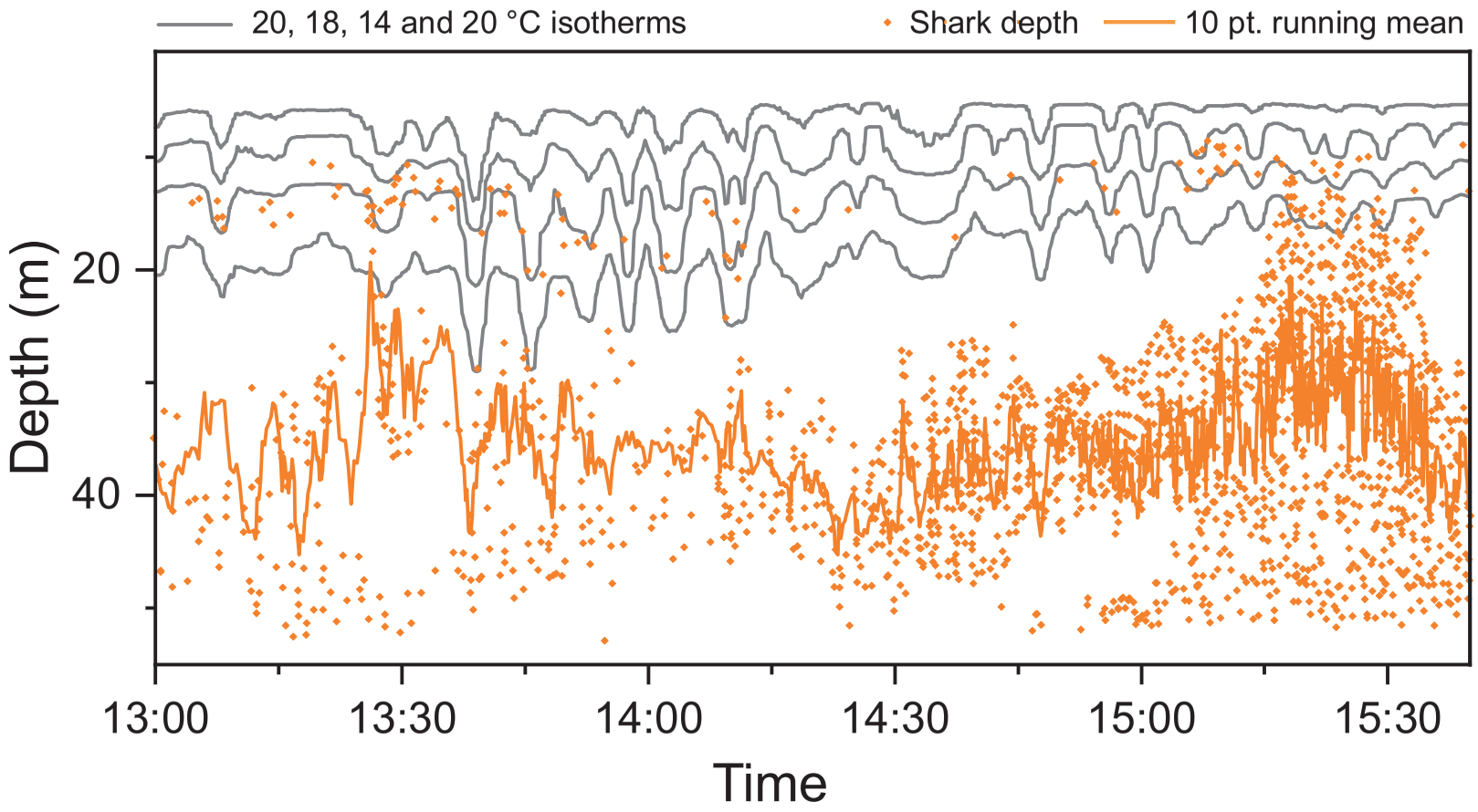

Fig.7 Shark depth Zmd and 20, 18, 14 and 10 °C isotherms on July 23

Online version

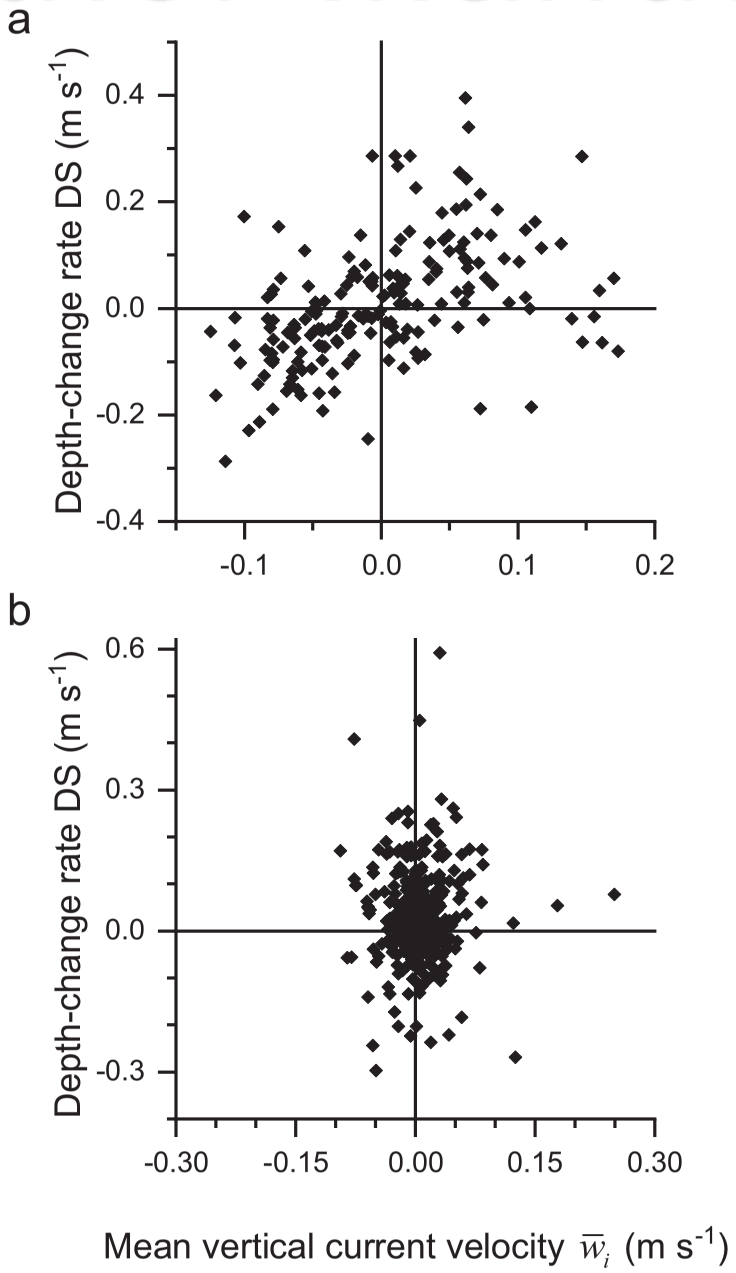

Fig. 8 Depth-change rate (DS) as a function of mean vertical currents, wi, on July 1. Individuals in (a) the steep and (b) non-steep regions of the NLIW.

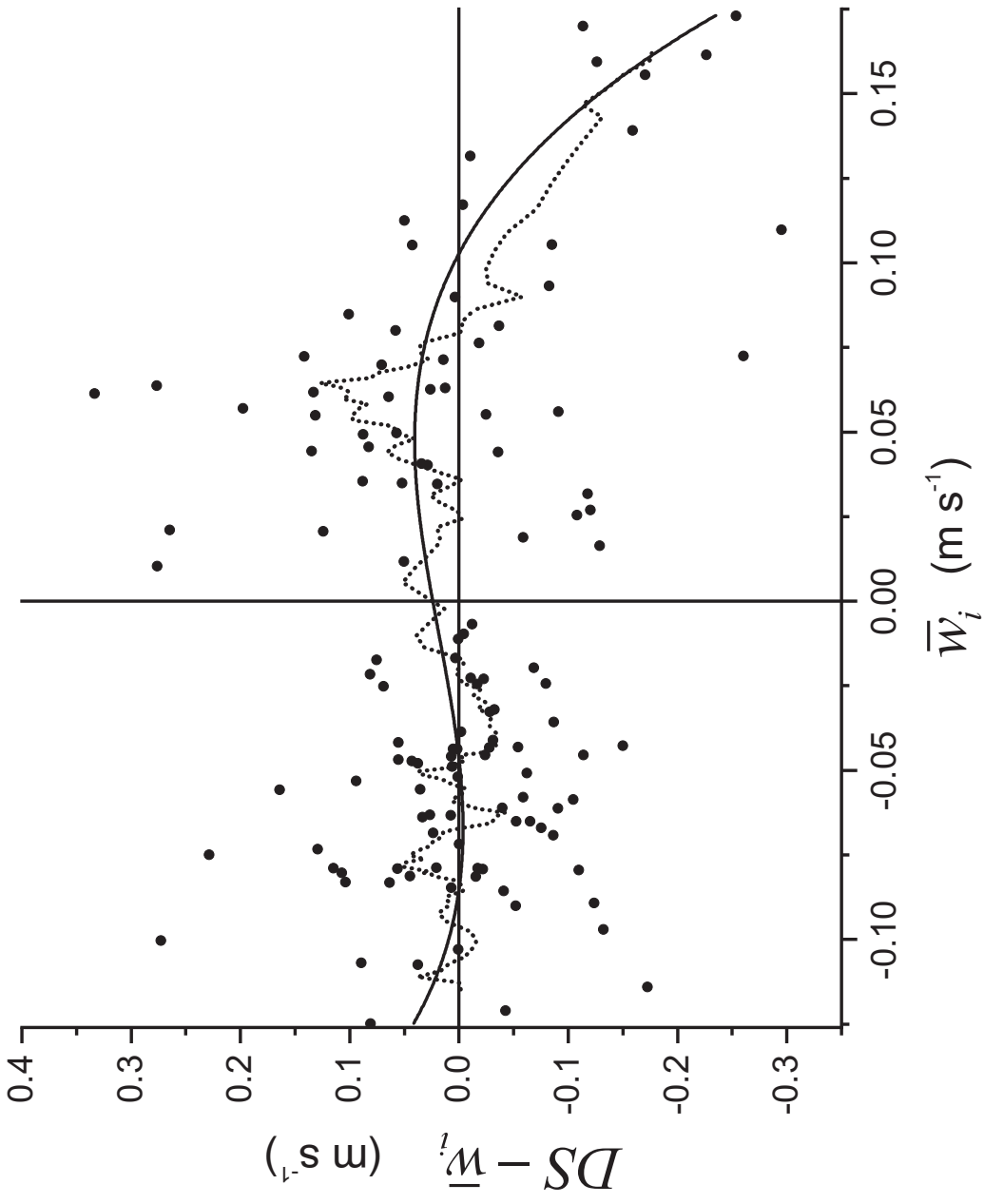

Fig. 9. DS with mean vertical currents wi removed as a function of wi, for traces in the steep section of the NLIW, 10-point running mean (dotted line), and cubic polynomial fit (solid line).

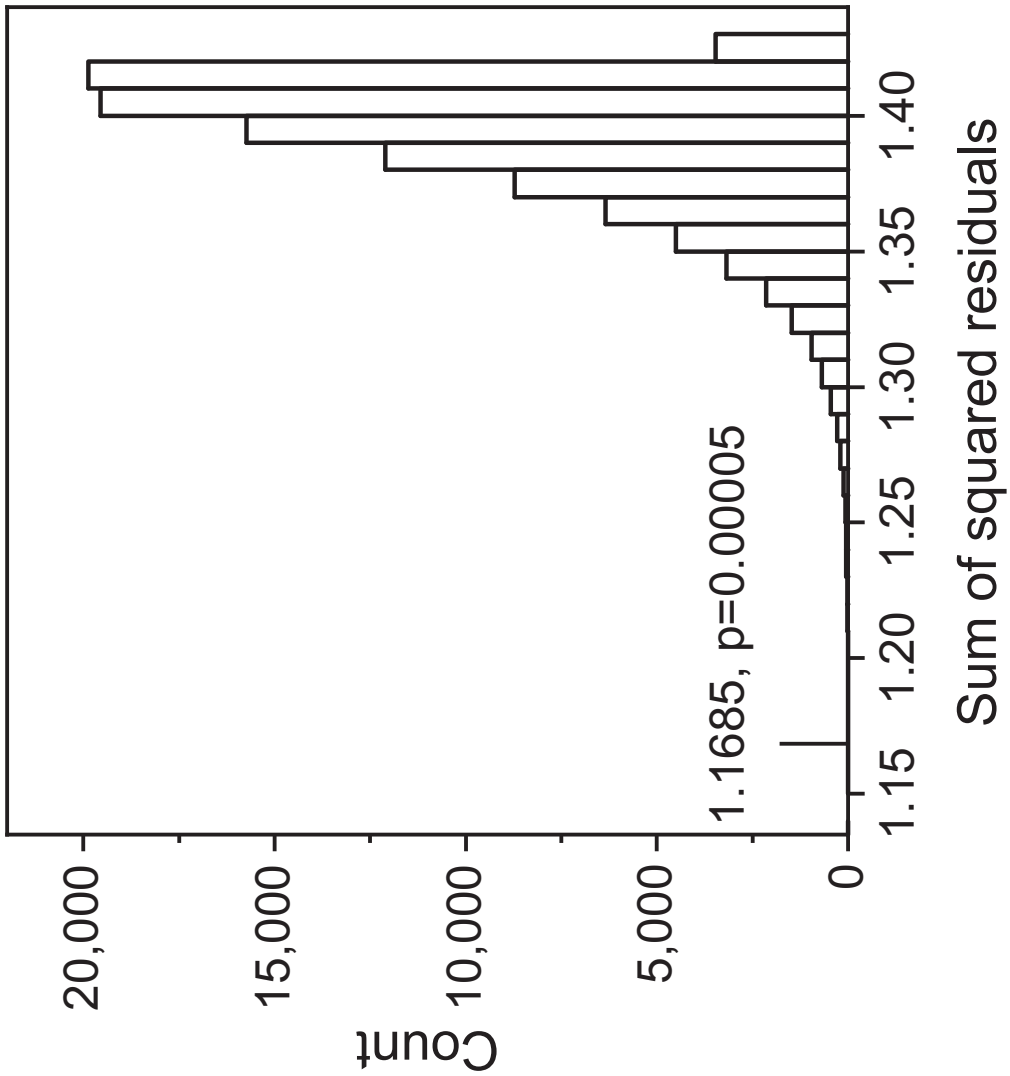

Fig. 10. Frequency distribution of the sum squared residuals (ssr) from cubic polynomial fit of 100,000 randomized DS - wi values. The ssr from the observed data and approximate p are also given.